


Nonadiabatic electron-phonon coupling and its effects on superconductivityShi-Qi Hu,^{1,2} Xin-Bao Liu ,^{1,2} Da-Qiang Chen,^{1,2} Chao Lian,¹ En-Ge Wang,^{1,3,4,5,*} and Sheng Meng^{1,2,3,†}¹*Beijing National Laboratory for Condensed Matter Physics and Institute of Physics, Chinese Academy of Sciences, Beijing 100190, China*²*School of Physical Sciences, University of Chinese Academy of Sciences, Beijing 100049, China*³*Songshan Lake Materials Laboratory, Dongguan, Guangdong 523808, China*⁴*International Center for Quantum Materials and School of Physics, Peking University, Beijing 100871, China*⁵*School of Physics, Liaoning University, Shenyang 110136, China*

(Received 23 March 2022; revised 29 May 2022; accepted 6 June 2022; published 23 June 2022)

As one of the most striking phenomena in many-body systems, the breakdown of the adiabatic Born-Oppenheimer (ABO) approximation is essential for understanding and predicting the dynamics of quantum materials. Here, we demonstrate that strong nonadiabatic (NA) effects can emerge in electron-phonon coupling (EPC) and resultant superconductivity, yielding a surprisingly large contribution (up to 20%) to the total EPC strength λ of doped graphene/graphane and modulating the superconductivity transition temperature T_c by $\sim 20\%$. The NA EPC, with a detectable isotopic effect, results from the renormalized EPC matrix elements (up to 40%) combined with the Fermi surface modulation, due to electron distributions deviating from the equilibrium. Our results imply that nonadiabaticity plays a wider and more important role than previously conceived, offering new understandings and strategies for dynamic engineering of quantum materials.

DOI: [10.1103/PhysRevB.105.224311](https://doi.org/10.1103/PhysRevB.105.224311)**I. INTRODUCTION**

The adiabatic Born-Oppenheimer (ABO) approximation, which assumes that the lighter electrons follow adiabatically the motion of heavier nuclei and remain in the ground state, has been the standard ansatz to describe the dynamics in many-body systems [1,2]. However, the ABO approximation fails when the energy gap between electronic states is close to the energy scale of the nuclear motions [3]. For a reliable understanding and prediction of the dynamics in metallic and narrow-band-gap quantum materials, the nonadiabaticity must be taken into account.

Recent studies have shown the impact of nonadiabatic (NA) effects in various physical behaviors, such as the NA pairing in superconductivity [4,5], the electronic correlation effects [6,7], and the phonon renormalization widely studied in layered and bulk materials [8–12]. The nonadiabaticity is also important in the proton-coupled electron transfer [13], which governs processes ranging from the photochemistry of molecules in the atmosphere to biological reactions such as vision.

Among these processes, the nonadiabaticity describes the feedback between electron dynamics and atomic motions: atomic vibrations lead to transitions between electronic states, which, in turn, alter the potential energy surfaces experienced by the atoms. This correlation between electronic and atomic dynamics naturally yields an open question about whether the nonadiabaticity has a significant influence on one of the

most fundamental interactions in materials, i.e., the electron-phonon couplings (EPC) and the relevant superconductivity, which are vital in power/particle transmission [14–16], electronics, and solar cell applications [17–19].

There is a clear breakdown of the ABO approximation in doped graphene and its derivative graphane [20–23], due to the low-dimensional nature, the gapless Dirac band structure [20], and high-frequency optical phonons at the Γ point [10], i.e., the E_{2g} (TO/LO mode) phonons whose energy is ~ 0.2 eV for graphene and ~ 0.1 eV for graphane. For graphene, it has been shown that the adiabatic approximation is totally broken down in previous theories and experiments [8,9]. As the derivative of graphene, doped graphane also has large NA effects, similar to the case of doped diamond, which has a strong NA Kohn anomaly [12]. More importantly, since the E_{2g} (TO/LO mode) phonons in doped graphene/graphane have the dominant contributions to the EPC and superconductivity, the study of these phonons in doped graphene/graphane would reveal the impact of nonadiabaticity on the superconductivity, which is significant both in the fundamental physics and real applications of condensed matter.

In the present work, the nonadiabaticity is investigated from the viewpoint of EPC and superconductivity in doped graphene/graphane based on real-time time-dependent density-functional theory (rt-TDDFT) [24–27]. Our advanced method naturally includes nonadiabaticity in the EPC matrix element, and it reveals that the nonadiabaticity has a vital contribution to the effective EPC strength λ (up to 20%) [28,29]. As a consequence, the prediction of superconductivity transition temperature T_c is expected to change by $\sim 20\%$ [30–34]. Since the EPC correlates electron and atom dynamics, the nonadiabaticity may also affect catalytic reactions at metal surfaces [35,36] and exciton dynamics [37,38] by shaping

* Author to whom all correspondence should be addressed: egwang@pku.edu.cn

† smeng@iphy.ac.cn

the electronic energy surfaces and driving transitions between them, which should be fully considered in many-body systems.

II. METHODS

The investigations are performed with state-of-the-art first-principles calculations, using the time-dependent *ab initio* package (TDAP) as implemented in SIESTA [39–41], which was developed recently to successfully describe nonequilibrium dynamics in solids [24]. In our simulations, numerical atomic orbitals with double zeta polarization are used as the basis set. The \mathbf{k} sampling in the Brillouin zone is a Γ -centered $144 \times 144 \times 1$ mesh. The electron-nuclear interactions are described by norm-conserving pseudopotentials with an energy cutoff of 100 Ry in the local-density approximation (LDA). For the lattice, we use the unit cell relaxed by SIESTA with a lattice parameter $a = 2.45 \text{ \AA}$ for graphene and $a = 2.54 \text{ \AA}$ for graphane. More details about the algorithm and parameters can be found in Refs. [39–41].

The atoms are initially stretched along the phonon eigenmode displacement and released to oscillate, to introduce phonon vibrations in the present study [42]. The atom displacement stretched along phonon eigenmode Δu is 0.5–1 % of the equilibrium bond length a_{C-C} , corresponding to the phonon amplitude at ~ 30 K. The adiabatic dynamics are simulated by ground-state molecular dynamics (MD). While for NA dynamics the electrons can be in excited states and have nonequilibrium distributions by scattering with phonons, the NA effects are included naturally by the rt-TDDFT molecular dynamics (rt-TDDFT-MD), which realizes the NA feedback between electrons and phonons through evolving both of them simultaneously. The electron dynamics are obtained by solving the time-dependent Kohn-Sham equation within the phonon bath, while the phonon dynamics are decided from time-dependent electron wave functions through the Hellmann-Feynman theorem.

III. EPC MATRIX FROM NONADIABATIC DYNAMICS

To quantify EPC, the effective EPC strength λ is obtained from [29,43,44]

$$\lambda = \sum_{\text{ph}} \frac{\langle g^2 \rangle_{\text{F}}}{N_{\text{f}} \hbar \omega_{\text{ph}}}, \quad (1)$$

where N_{f} is the density of states (DOS) at the Fermi surface (FS), and $\hbar \omega_{\text{ph}}$ is the phonon energy. Σ_{ph} is the sum among different phonon modes. $\langle g^2 \rangle_{\text{F}} = \left(\frac{2\hbar}{M\omega_{\text{ph}}}\right)^{1/2} \sum_{i,j,k}^{\text{FS}} |g_{i,j}(k, q)|^2 / N_k$ is the square sum of EPC matrix elements on FS, and $g_{ij}(k, q)$ is the EPC matrix element with k electron momentum and q phonon momentum. The i and j are the indexes of electronic eigenstates, since $g_{ij}(k, q) = \langle \varphi_i | \partial V(k, q) / \partial u | \varphi_j \rangle$, where $\langle \varphi_i |$ and $\langle \varphi_j |$ are the wave functions of the i th and j th electronic eigenstates. u and $V(k, q)$ are the atom displacement and corresponding deformation potential [28,29]. The phonon mode dependence of $\langle g^2 \rangle_{\text{F}}$ is described by the phonon frequency term ω_{ph} and $g_{ij}(k, q)$. The average of the sum of the square of EPC matrix

elements on FS is taken into account by N_k , which denotes the number of \mathbf{k} points on the FS contributing $\langle g^2 \rangle_{\text{F}}$.

Since the NA effects mainly affect the optical phonon modes at the Γ point (denoted here as E_{2g} phonon@ Γ) [10], the phonon momentum q here is zero in the $\langle g^2 \rangle_{\text{F}}$ equation. As shown in Eq. (2) of the previous study [44], for Γ point phonons in doped graphene, the diagonal term of EPC matrix elements on π^* band $g_{k\pi^*,k\pi^*}$ [in our work it is $g_{ii}(k)$] plays dominant roles in the EPC. Therefore, we mainly focus on $g_{ii}(k)$ in our study.

The g_{ii} of the i th band can be represented as the first derivative of the band energy E_i at each \mathbf{k} point with respect to atomic displacement Δu , i.e., $g_{ii} = \partial E_i / \partial u = \Delta E_i / \Delta u$. Δu is the stretched atom displacement and ΔE_i is the corresponding band energy change between the original relaxed lattice and the stretched lattice, respectively. Within an adiabatic framework, ΔE_i is obtained from the vibration of atoms, while the electrons remain in the ground-state configuration, i.e., the ground-state frozen-phonon approach. By contrast, in a nonadiabatic framework, the ΔE_i has two contributions. One is the same vibration of structure as in the adiabatic case. The other is the nonequilibrium electronic configuration due to the transition caused by the scattering with phonons, which *cannot* be described with the ABO approximation. More details on the calculation methods can be found in the supplemental material [45]. Here we mainly focus on the relative comparison of EPC between the adiabatic and nonadiabatic frameworks. This comparison is expected to be effective even with the *GW* regime.

IV. NONADIABATICITY-INDUCED PHONON RENORMALIZATION

We first investigate the nonadiabaticity-induced phonon renormalization in doped graphene with the E_{2g} phonon@ Γ ($\hbar \omega_{E_{2g}} \approx 0.2 \text{ eV}$). In Fig. 1(a), we display the frequency shift of E_{2g} phonon@ Γ as a function of doping concentration in both adiabatic and NA simulations. The doping concentration is tuned by adding electrons/holes and is described by the Fermi energy shift $\pm (E_{\text{f}} - E_{\text{D}})$, where E_{f} is the energy level of FS with a particular value of the doping concentration in an equilibrium ground state, and E_{D} is the energy level of the Dirac point. For the undoped case, $E_{\text{f}} = E_{\text{D}}$. The + (–) sign labels the increasing (decreasing) electron concentration. The NA effects cause the anomalous phonon softening through EPC [9,21–23,46], and the results with NA simulations show good consistency with the experiments [22,23], implying our TDDFT dynamics retrieve the NA features completely.

V. THE NONADIABATIC EFFECTS ON EPC

We then go further to explore the NA effects on EPC. According to Eq. (1), the EPC strength is determined by the sum of EPC matrix elements squared $\langle g^2 \rangle_{\text{F}}$. On the one hand, the NA effects mainly occur on the high-frequency optical phonons at the Γ point (in graphene, it is the E_{2g} phonon@ Γ). On the other hand, the E_{2g} phonon@ Γ has a significant contribution to the total EPC in graphene. The NA

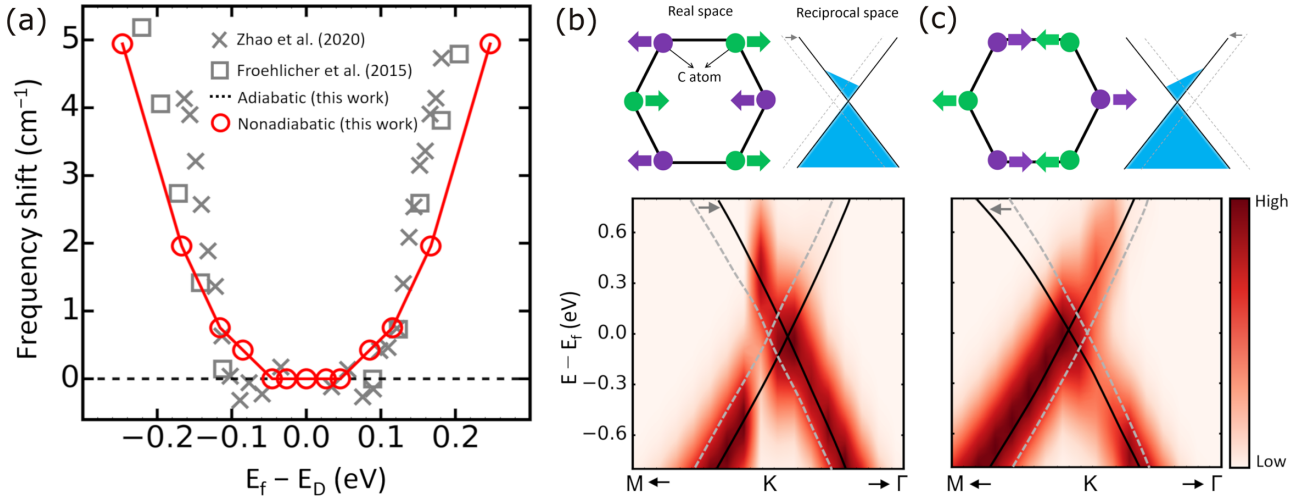


FIG. 1. (a) The evolution of the E_{2g} phonon@ Γ energy with doping concentrations [represented by $\pm(E_f - E_D)$] in graphene. The black dashed line and the red solid line in (a) show the adiabatic and NA results, respectively. The gray labels mark the experimental measurements from Zhao *et al.* [22] and Froehlicher *et al.* [23]. (b),(c) Schematics showing the vibration pattern of atoms and NA oscillation of Dirac cones in the presence of E_{2g} phonon@ Γ in electron-doped graphene (top). Regions with blue shading are filled with electrons. The snapshots for the TDDFT-simulated oscillation of Dirac cones and the corresponding electron distribution (bottom). The red regions are occupied by electrons. The NA effect can be clearly seen from the slanting electron occupation and the oscillation delay between the electrons and Dirac cones. The dashed gray and solid black lines in (b) and (c) label the Dirac cone positions with atom displacement $u_0 = 0$ and $1\% \times a_{C-C}$, respectively. The gray arrows show the oscillation directions (along Γ - K - M).

effects on E_{2g} phonon@ Γ would thus have vital modulations on EPC. Therefore, here we mainly focus on contributions by E_{2g} phonon@ Γ : $\langle g_{ii}^2 \rangle_F = \left(\frac{2\hbar}{M\omega_{E_{2g}}} \right)^{1/2} \sum_{ik}^{FS} |g_{ii}(k)|^2 / N_k$ [43,44], which is summed on the FS of the π^* band of a Dirac cone. The definition indicates the FS configuration and EPC matrix element g_{ii} play vital roles in determining the EPC. Therefore, the nonadiabaticity can affect the EPC by modulating FS and renormalizing g_{ii} [12,47]. We will discuss them in the following. For DOS and phonon energy in Eq. (1), the NA effects on them are not involved [48]. Taking the doping level at $|E_f - E_D| \sim 0.24$ eV as an example, the ratio between energy shift and initial phonon energy $\Delta\hbar\omega_{E_{2g}}/\hbar\omega_{E_{2g}}^0$ is $\sim 0.3\%$, which is negligible when dealing with EPC strength.

VI. NONADIABATICITY-MODULATED FERMI SURFACE

As shown in Figs. 1(b) and 1(c), for doped graphene, with E_{2g} phonon@ Γ the atoms are displaced from the equilibrium positions and oscillate along the carbon-carbon bond. The Dirac cones oscillate correspondingly along the Γ - K - M direction in the reciprocal space due to the lattice distortion [9]. Within the ABO approximation, the carriers (electrons/holes) on the Dirac cones move together with the bands and stay in the ground state at any time during the oscillation. The FS follows the Dirac cone displacement and stays constant (horizontal) in energy.

However, considering the nonadiabaticity, the carriers driven by phonon oscillations have no time to fully relax to the ground state and show a nonequilibrium occupation, so there is a clear delay between the oscillation of carriers, Dirac cones, and phonons (see also Fig. S1 in Ref. [45]). The FS *cannot* follow closely the Dirac cone displacement

and becomes slanting [9]. This statement is confirmed by our TDDFT simulations from which the snapshots during the oscillation are shown at the bottom of Figs. 1(b) and 1(c). Moreover, due to the zero band gap of Dirac cones, the nonadiabaticity provides phonon-assisted transition channels for carriers in graphene. The above two aspects make the electron distribution in energy and momentum space no longer homogeneous and out of equilibrium [9], which perturbs the FS. Therefore, an “effective” nonequilibrium FS is formed after considering the nonadiabaticity.

As exhibited in Fig. 2(a), in electron-doped graphene ($|E_f - E_D| \sim 0.24$ eV) the nonequilibrium FS modulated by NA effects is represented by the outline of electron occupation fluctuation on π^* bands (red solid-lined ring). The nonadiabaticity-modulated FS is mainly located along the K - M direction in response to the motion of E_{2g} phonon@ Γ , different from that under the ABO approximation (the range denoted by the black dash-lined ring).

The corresponding distribution of the adiabatic EPC matrix element of the π^* band $|g_{ii}^A|$ (here we use the absolute value to quantify the intensity) in the Brillouin zone is shown in Figs. 2(b) and 2(c). Unlike the band structure, the EPC matrix element $|g_{ii}^A|$ has an anisotropic distribution, where the K - M and K - M' paths become nondegenerate due to the broken hexagonal symmetry induced by the phonon. Note that the strong and dominant $|g_{ii}^A|$ is mainly distributed along the K - M direction, which is the same as the nonadiabaticity-modulated FS. That means compared to the adiabatic equilibrium FS, the EPC matrix element on the nonadiabaticity-modulated nonequilibrium FS would have a higher intensity. Since the EPC strength is proportional to the sum of the EPC matrix element squared on the FS, the nonadiabaticity would promote the EPC by modulating the FS to the area where strong $|g_{ii}^A|$ is located.

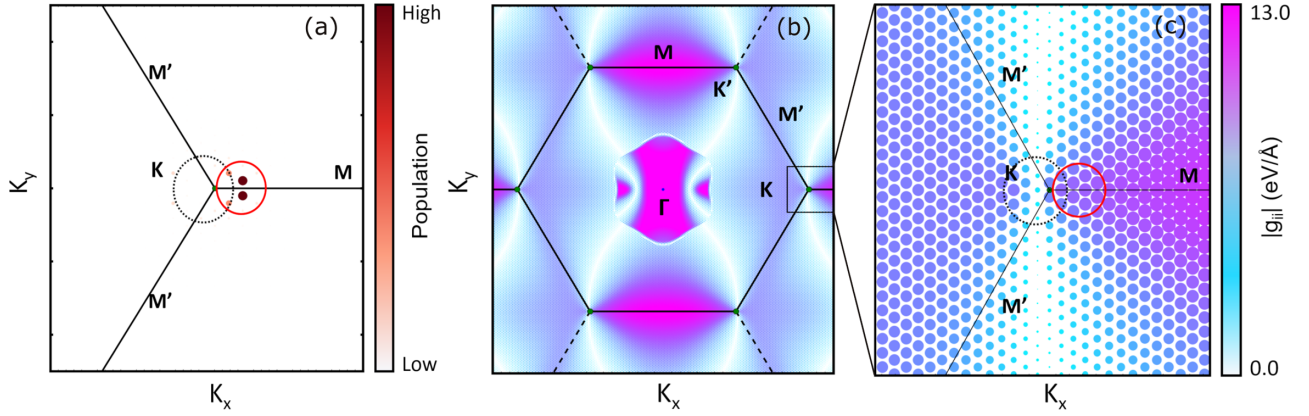


FIG. 2. (a) The distribution of the electron occupation fluctuation on π^* bands around the Dirac point in reciprocal space of doped graphene, in response to the motion of E_{2g} phonon@ Γ . The electron distribution forms an effective nonequilibrium FS (red solid ring) that is different from the adiabatic case (black dashed ring). (b) The distribution of the adiabatic EPC matrix element of π^* bands $|g_{ii}^A|$ in the Brillouin zone of doped graphene. (c) The distribution of $|g_{ii}^A|$ around the Dirac point. The black dashed rings in (a) and (c) label the adiabatic equilibrium FS. The color and size of the circles in (a) and (c) represent the values of electron population and $|g_{ii}^A|$, respectively.

VII. NONADIABATICITY-RENORMALIZED EPC MATRIX

The nonadiabaticity affects the deformation potential V by dressing the electron distributions out of equilibrium and thus renormalizes the EPC matrix element itself. In Fig. 3(a) we plot the strength difference of EPC matrix element $\Delta g_{ii} =$

$|g_{ii}^{\text{NA}}| - |g_{ii}^A|$ of π^* bands around the Dirac point in doped graphene ($|E_f - E_D| \sim 0.24$ eV, where g_{ii}^{NA} (g_{ii}^A) is the EPC matrix element in an NA (adiabatic) framework. Since the Dirac cones oscillate along the Γ - K - M direction (k_x direction), the symmetry of the Δg_{ii} distribution is broken along the

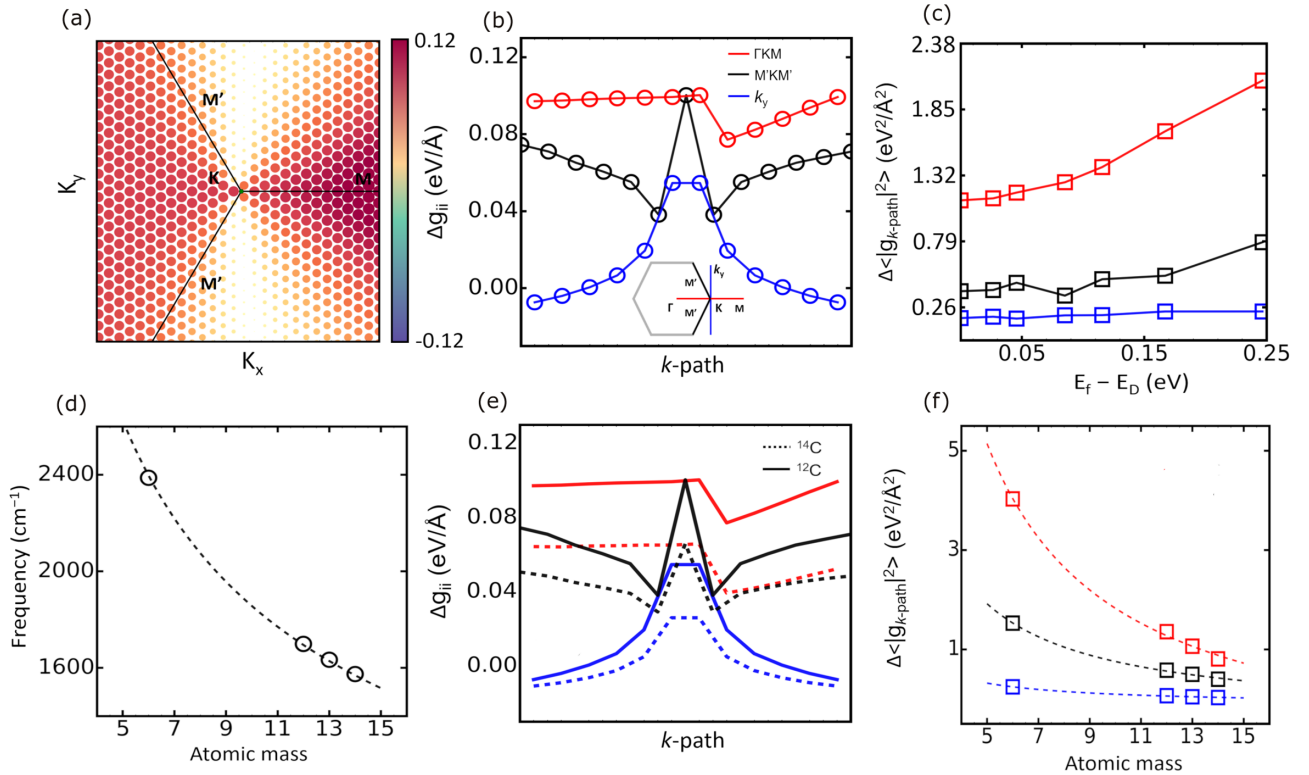


FIG. 3. (a) The distribution of Δg_{ii} around the Dirac point in the Brillouin zone of doped graphene. $\Delta g_{ii} = |g_{ii}^{\text{NA}}| - |g_{ii}^A|$ is the difference between adiabatic and nonadiabatic EPC matrix elements of π^* bands. The color and size of the circles represent the value of Δg_{ii} . (b) The distribution of Δg_{ii} along different k -paths. (c) $\Delta \langle |g_{k\text{-path}}|^2 \rangle$ as a function of doping concentrations [represented by $\pm(E_f - E_D)$] along different k -paths. As shown in the inset of (b), the gray hexagon shows the first Brillouin zone of graphene. The red, black, and blue lines represent the k -path along Γ - K - M , M' - K - M' , and k_y , respectively. (d) The phonon frequency as a function of the atomic mass of C isotope. (e) The distribution of Δg_{ii} along different k -paths of graphene formed by ^{12}C and ^{14}C isotopes. (f) $\Delta \langle |g_{k\text{-path}}|^2 \rangle$ as a function of the atomic mass of C isotope. The dashed lines in (d) and (f) are fitted by $\sim 1/m$, and m is the atomic mass.

k_x direction and maintained along the perpendicular direction (k_y direction), showing an anisotropy in the Brillouin zone. It should be noted that around the Dirac points, almost all the Δg_{ii} are positive (the slightly negative values exist only in a small range along the k_y direction), indicating that the NA effect amplifies the g_{ii} , where the averaged nonadiabaticity ratio $\Delta g_{ii}/|g_{ii}^A|$ is $\sim 1\%$ in doped graphene (we note that this ratio $\Delta g_{ii}/|g_{ii}^A|$ can reach $\sim 40\%$ for doped graphane, as discussed later).

In Fig. 3(b), the nonadiabaticity-renormalized Δg_{ii} of π^* bands shows a k -path dependence. The dominant enhancement of Δg_{ii} is along the Γ - \mathbf{K} - \mathbf{M} path, the same direction of Dirac cone oscillation and FS slanting [Figs. 1(a) and 1(b)] where the nonadiabaticity is most significant. We also investigate the g_{ii} in larger supercells, which enable more channels for electron and phonon scatterings, and we obtain similar results.

In Fig. 3(c) we compare the NA effects on the sum of squared EPC matrix elements by $\Delta \langle |g_{k\text{-path}}|^2 \rangle = \langle |g_{k\text{-path}}^{\text{NA}}|^2 \rangle - \langle |g_{k\text{-path}}^{\text{A}}|^2 \rangle$ along different k -paths. Here $\langle |g_{k\text{-path}}^{\text{NA/A}}|^2 \rangle = \sum_{k\text{-path}} |g_{ii}^{\text{NA/A}}(k)|^2 / N_{k\text{-path}}$ denotes the sum of the NA/adiabatic squared EPC matrix element $g_{ii}^{\text{NA/A}}$ along the special k -path, and $N_{k\text{-path}}$ is the number of k points along the special k -path. Due to the significant nonadiabaticity along the Γ - \mathbf{K} - \mathbf{M} path, the NA contribution $\Delta \langle |g_{k\text{-path}}|^2 \rangle$ along this direction becomes dominant. Moreover, with the increase in the doping concentration, the energy difference of electrons between the nonadiabatic and adiabatic cases is enhanced [9] and thus $\Delta \langle |g_{k\text{-path}}|^2 \rangle$ increases with $|E_f - E_D|$.

Since the nonadiabaticity is dependent on atomic mass, we investigate the measurable isotope effect on the nonadiabaticity-renormalized EPC by artificially changing the atomic mass. As shown in Fig. 3(e), though the NA modulation Δg_{ii} has a similar k -path dependence for ^{12}C and ^{14}C , the lighter ^{12}C has a higher Δg_{ii} value. Similar trends can also be found on the phonon frequency and $\Delta \langle |g_{k\text{-path}}|^2 \rangle$ along a different k -path as a function of the atomic mass of C [Figs. 3(d) and 3(f)]. Both of them show a $1/m$ relationship as the atomic mass m increases, showing consistency with the statement that the NA effects will be more significant with the lighter atom mass.

The results of graphene in Figs. 2 and 3 demonstrate that the nonadiabaticity has nontrivial effects on both the FS and the EPC matrix. As a consequence, $\langle g_{\Gamma}^2 \rangle_{\text{F}}$ increases with doping level in graphene (Fig. S2 [45]). Such effects were neglected in previous treatments based on density functional perturbation theory (DFPT), where $\langle g_{\Gamma}^2 \rangle_{\text{F}} \sim 0.04 \text{ eV}^2$ is equilibrated and constant [43,44].

Moreover, in the previous studies the NA effects on EPC are usually described based on the perturbation theory by the unscreened EPC matrix elements $g_{ii}^b = g_{ii}^A / \epsilon_r(\omega_{\text{ph}})$, where $\epsilon_r(\omega_{\text{ph}})$ is the dielectric function at phonon frequency [12,28]. We compare our results directly with the g_{ii}^b (Fig. S3 [45]) in graphene. The results show that the unscreened $|g_{ii}^b|$, as an ad-hoc approach, significantly overestimates the NA effects by removing electron screening altogether, while in real situations the nonadiabaticity affects a part of the electrons fluctuating near the FS.

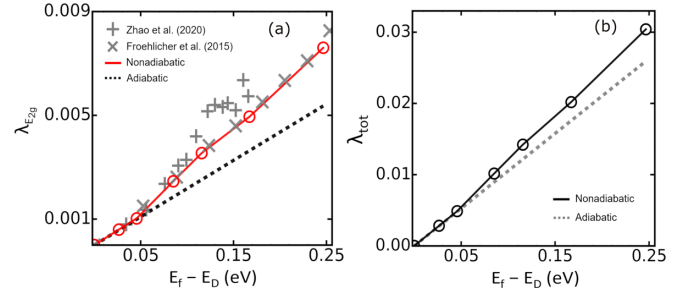


FIG. 4. (a) The EPC strength $\lambda_{E_{2g}}$ contributed by E_{2g} phonon@ Γ as a function of doping concentrations (represented by $E_f - E_D$). The black dashed and red solid lines label the adiabatic and NA results, respectively. The gray labels mark the $\lambda_{E_{2g}}$ retrieved from experimental data by Zhao *et al.* [22] and Froehlicher *et al.* [23]. (b) The total EPC strength λ_{tot} contributed by E_{2g} phonon@ Γ and A'_1 phonon@ \mathbf{K} as a function of doping concentrations. The dashed and solid lines label the adiabatic and NA results, respectively.

Based on Eq. (2) and deductions in Ref. [44], we calculate the EPC strength $\lambda_{E_{2g}}$ contributed by E_{2g} phonon@ Γ in graphene including the two NA contributions mentioned earlier (the nonadiabaticity-modulated FS and renormalized g_{ii}) [48]. The $\lambda_{E_{2g}}$ as a function of doping concentrations is shown in Fig. 4(a). Compared to the EPC strength under the ABO approximation $\lambda_{E_{2g}}^{\text{A}}$, the EPC strength with NA effects $\lambda_{E_{2g}}^{\text{NA}}$ shows better agreement with the results retrieved from experimental data [22,23]. Only after considering the nonadiabaticity could we obtain a good agreement of λ between theory and experiment.

Since the total EPC in graphene is mainly contributed by E_{2g} phonon@ Γ and A'_1 phonon@ \mathbf{K} , we include both E_{2g} phonon@ Γ and A'_1 phonon@ \mathbf{K} to investigate the NA effects on total EPC strength λ_{tot} . The A'_1 phonon is introduced by using the $\sqrt{3} \times \sqrt{3}$ supercell and assuming that the nonadiabaticity has negligible effects on the A'_1 phonon, which is verified by our simulations. The EPC matrix of the A'_1 phonon is then obtained from DFPT, and the total EPC λ_{tot} in graphene is calculated using Eq. (15) in Ref. [44], with $\langle g_{\mathbf{K}}^2 \rangle_{\text{F}} \sim 0.1 \text{ eV}^2$ and $\hbar\omega_{A'_1} \sim 0.16 \text{ eV}$ [44]. As shown in Fig. 4(b), taking the A'_1 phonon into account does not change our major conclusion, namely, the nonadiabaticity has a large enhancement on the total λ in graphene. At the doping of 0.24 eV, the NA enhancement of λ_{tot} is $\sim 15\%$, which shows a giant impact on electron-phonon interactions.

VIII. NONADIABATIC EFFECT ON SUPERCONDUCTIVITY

One consequence of nonadiabaticity on EPC is the modification of the superconductivity transition temperature T_c . Since the EPC strength λ in graphene is too small to give a reliable T_c , we choose hydrogenated graphene (graphane) as the example, which is shown to be a stable high-temperature EPC superconductor with hole doping [34]. The strong EPC in graphane is mainly contributed by the in-plane optical E_{2g} phonons@ Γ (TO modes). The EPC strength λ and T_c in the

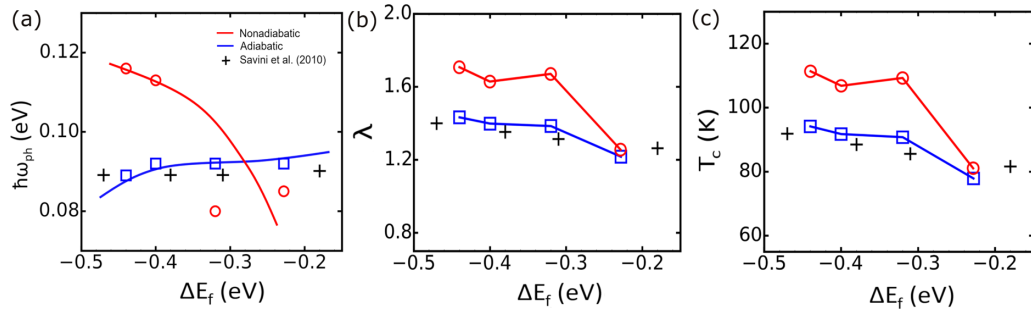


FIG. 5. The TO phonon frequency (a), total EPC strength λ (b), and superconducting transition temperature T_c (c) as a function of hole doping (represented by ΔE_f) in graphane, with and without the NA effects.

adiabatic/NA cases are calculated by Eq. (1) and McMillan's formula [45,49,50].

As shown in Fig. 5, the phonon frequency, total EPC strength λ , and superconducting transition temperature T_c are plotted as a function of hole doping level (represented by ΔE_f) in graphane, with and without the NA effects.

As the doping level increases, the phonon frequency is redshifted in the adiabatic approximation while blueshifted in the NA case, showing the obvious phonon energy renormalization (up to 30%). The adiabatic λ and T_c agree well with the previous results [34]. Interestingly, the NA effects can also enhance λ and T_c . The doping dependence of NA EPC and T_c originates from the phonon energy renormalization and EPC matrix modulated by the nonadiabaticity. As shown in Fig. S5 [45], taking $\Delta E_f = -0.45$ eV as the example, the nonadiabaticity has a positive contribution to the g_{ii} around Fermi level; the NA ratio $|\Delta g_{ii}/g_{ii}^A|$ is $\sim 40\%$. The nonadiabaticity enhances the λ and T_c by $\sim 20\%$, indicating a significant effect on EPC and superconductivity.

IX. DISCUSSION

The advanced methodology (TDDFT) we used naturally includes nonadiabaticity in the electron-phonon interaction process and enables us to do the following: (i) To explore directly the microscopic dynamics on nonadiabaticity-induced nonequilibrium distribution of electrons on a Dirac cone, which is only given as a speculative schematic picture in a previous study [9], and reveal the NA phase of the band oscillation (Fig. S1 [45]). (ii) To reveal the giant NA effect on the EPC itself and provide the mechanism behind it (the nonadiabaticity-induced EPC matrix elements renormalization and the FS modulation). This is also the main difference between our study and previous works, which focus on the NA self-energy correction on phonon frequency while the NA EPC is always neglected and assumed to take the adiabatic value calculated from the ABO approximation [9,12,21]. (iii) To exhibit and give clear clues on the nontrivial isotopic effect

of NA effects, which is also rarely discussed in previous studies.

Since the NA effects are dependent on atomic mass, a similar nonadiabaticity on EPC may strongly beacon itself in hydrogen-based superconductors possessing near-room-temperature T_c 's under high pressures [51,52]. These results remind us that the nonadiabaticity should be fully considered in electron-phonon interaction dominated materials.

X. CONCLUSION

In conclusion, we demonstrate that the nonadiabaticity not only modulates electron distribution and thus FS, but also contributes significantly to the EPC matrix element renormalization, which can reach 40% and exhibit a strong anisotropy in the Brillouin zone. Consequently, the nonadiabaticity can contribute to the EPC strength λ and modulate the superconductivity transition temperature T_c by $\sim 20\%$, taking doped graphene/graphane as examples. Our results reveal the universality and significance of nonadiabaticity in many-body systems, opening new doors for the dynamic engineering of quantum materials. We expect that similar NA effects may appear in other systems, such as multivalley solids [47,53] and Dirac/Weyl materials [54].

ACKNOWLEDGMENTS

We acknowledge financial support from MOST (Grant No. 2021YFA1400200), NSFC (Grants No. 12025407, No. 11934003, No. 91850120, and No. 11774328), and CAS (XDB330301).

S.M. and E.W. conceived and supervised the project. S.-Q.H. and X.-B.L. performed the theoretical modeling and TDDFT calculations. D.-Q.C. and C.L. contributed to the software code. S.-Q.H., X.-B.L., D.-Q.C., and S.M. analyzed the data. The manuscript was written by S.-Q.H. and S.M. with input from all authors.

- [1] M. Born and J. R. Oppenheimer, Zur quantentheorie der molekeln, *Ann. Phys.* **84**, 457 (1927).
- [2] J. M. Ziman, *Electrons and Phonons* (Oxford University Press, Oxford, 1960).
- [3] S. Engelsberg and J. R. Schrieffer, Coupled electron-phonon system, *Phys. Rev.* **131**, 993 (1963).

- [4] E. Cappelluti, S. Ciuchi, C. Grimaldi, L. Pietronero, and S. Strässler, High T_c Superconductivity in MgB_2 by Nonadiabatic Pairing, *Phys. Rev. Lett.* **88**, 117003 (2002).
- [5] L. P. Gor'kov, Phonon mechanism in the most dilute superconductor n-type SrTiO_3 , *Proc. Natl. Acad. Sci. USA* **113**, 4646 (2016).

- [6] S. Gerber, S.-L. Yang, D. Zhu, H. Soifer, J. A. Sobota, S. Rebec, J. J. Lee, T. Jia, B. Moritz, C. Jia, A. Gauthier, Y. Li, D. Leuenberger, Y. Zhang, L. Chaix, W. Li, H. Jang, J.-S. Lee, M. Yi, G. L. Dakovski *et al.*, Femtosecond electron-phonon lock-in by photoemission and x-ray free-electron laser, *Science* **357**, 71 (2017).
- [7] Z. P. Yin, A. Kutepov, and G. Kotliar, Correlation-Enhanced Electron-Phonon Coupling: Applications of GW and Screened Hybrid Functional to Bismuthates, Chloronitrides, and Other High- T_c Superconductors, *Phys. Rev. X* **3**, 021011 (2013).
- [8] M. Lazzeri and F. Mauri, Nonadiabatic Kohn Anomaly in a Doped Graphene Monolayer, *Phys. Rev. Lett.* **97**, 266407 (2006).
- [9] S. Pisana, M. Lazzeri, C. Casiraghi, K. S. Novoselov, A. K. Geim, A. C. Ferrari, and F. Mauri, Breakdown of the adiabatic Born-Oppenheimer approximation in graphene, *Nat. Mater.* **6**, 198 (2007).
- [10] A. M. Saitta, M. Lazzeri, M. Calandra, and F. Mauri, Giant Nonadiabatic Effects in Layer Metals: Raman Spectra of Intercalated Graphite Explained, *Phys. Rev. Lett.* **100**, 226401 (2008).
- [11] J. W. Quilty, S. Lee, A. Yamamoto, and S. Tajima, Superconducting Gap in MgB_2 Electronic Raman Scattering Measurements of Single Crystals, *Phys. Rev. Lett.* **88**, 087001 (2002).
- [12] F. Caruso, M. Hoesch, P. Achatz, J. Serrano, M. Krisch, E. Bustarret, and F. Giustino, Nonadiabatic Kohn Anomaly in Heavily Boron-Doped Diamond, *Phys. Rev. Lett.* **119**, 017001 (2017).
- [13] S. Hammes-Schiffer and A. V. Soudackov, Proton-coupled electron transfer in solution, proteins, and electrochemistry, *J. Phys. Chem. B* **112**, 14108 (2008).
- [14] P. B. Allen, Theory of Thermal Relaxation of Electrons in Metals, *Phys. Rev. Lett.* **59**, 1460 (1987).
- [15] C. H. Park, N. Bonini, T. Sohier, G. Samsonidze, B. Kozinsky, M. Calandra, F. Mauri, and N. Marzari, Electron-Phonon interactions and the intrinsic electrical resistivity of graphene, *Nano Lett.* **14**, 1113 (2014).
- [16] T. Y. Kim, C. H. Park, and N. Marzari, The electronic thermal conductivity of graphene, *Nano Lett.* **16**, 2439 (2016).
- [17] M. M. Lee, J. Teuscher, T. Miyasaka, T. N. Murakami, and H. J. Snaith, Efficient hybrid solar cells based on meso-structured organometal halide perovskites, *Science* **338**, 643 (2012).
- [18] W. S. Yang, J. H. Noh, N. J. Jeon, Y. C. Kim, S. Ryu, J. Seo, and S. I. Seok, High-performance photovoltaic perovskite layers fabricated through intramolecular exchange, *Science* **348**, 1234 (2015).
- [19] H. J. Snaith, Present status and future prospects of perovskite photovoltaics, *Nat. Mater.* **17**, 372 (2018).
- [20] A. H. Castro Neto, F. Guinea, N. M. R. Peres, K. S. Novoselov, and A. K. Geim, The electronic properties of graphene, *Rev. Mod. Phys.* **81**, 109 (2009).
- [21] J. Yan, Y. Zhang, P. Kim, and A. Pinczuk, Electric Field Effect Tuning of Electron-Phonon Coupling in Graphene, *Phys. Rev. Lett.* **98**, 166802 (2007).
- [22] Y. Zhao, L. Du, W. Yang, C. Shen, J. Tang, X. Li, Y. Chu, J. Tian, K. Watanabe, T. Taniguchi, R. Yang, D. Shi, Z. Sun, and G. Zhang, Observation of logarithmic Kohn anomaly in monolayer graphene, *Phys. Rev. B* **102**, 165415 (2020).
- [23] G. Froehlicher and S. Berciaud, Raman spectroscopy of electrochemically gated graphene transistors: Geometrical capacitance, electron-phonon, electron-electron, and electron-defect scattering, *Phys. Rev. B* **91**, 205413 (2015).
- [24] W. Ma, J. Zhang, L. Yan, Y. Jiao, Y. Gao, and S. Meng, Recent progresses in real-time local-basis implementation of time dependent density functional theory for electron-nucleus dynamics, *Comput. Mater. Sci.* **112**, 478 (2016).
- [25] M. Noda, S. A. Sato, Y. Hirokawa, M. Uemoto, T. Takeuchi, S. Yamada, A. Yamada, Y. Shinohara, M. Yamaguchi, K. Iida, I. Floss, T. Otobe, K.-M. Lee, K. Ishimura, T. Boku, G. F. Bertsch, K. Nobusada, and K. Yabana, SALMON: Scalable Ab-initio light-matter simulator for optics and nanoscience, *Comput. Phys. Commun.* **235**, 356 (2019).
- [26] C. D. Pemmaraju, F. D. Vila, J. J. Kas, S. A. Sato, J. J. Rehr, K. Yabana, and D. Prendergast, Velocity-gauge real-time TDDFT within a numerical atomic orbital basis set, *J. Comput. Phys. Commun.* **226**, 30 (2018).
- [27] N. Tancogne-Dejean, O. D. Mucke, F. X. Kartner, and A. Rubio, Impact of the Electronic Band Structure in High-Harmonic Generation Spectra of Solids, *Phys. Rev. Lett.* **118**, 087403 (2017).
- [28] F. Giustino, Electron-phonon interactions from first principles, *Rev. Mod. Phys.* **89**, 015003 (2017).
- [29] G. Grimvall, *The Electron-Phonon Interaction in Metals*, edited by E. Wohlfarth (North-Holland, New York, 1981).
- [30] J. S. Kim, L. Boeri, J. R. O'Brien, F. S. Razavi, and R. K. Kremer, Superconductivity in Heavy Alkaline-Earth Intercalated Graphites, *Phys. Rev. Lett.* **99**, 027001 (2007).
- [31] G. Profeta, M. Calandra, and F. Mauri, Phonon-mediated superconductivity in graphene by lithium deposition, *Nat. Phys.* **8**, 131 (2012).
- [32] B. M. Ludbrook, G. Levy, P. Nigge, M. Zonno, M. Schneider, D. J. Dvorak, C. N. Veestra, S. Zhdanovich, D. Wong, P. Dosanjh, C. Straßer, A. Stöhr, S. Forti, C. R. Ast, U. Starke, and A. Damascelli, Evidence for superconductivity in Li-decorated monolayer graphene, *Proc. Natl. Acad. Sci. USA* **111**, 11795 (2015).
- [33] S.-L. Yang, J. A. Sobota, C. A. Howard, C. J. Pickard, M. Hashimoto, D. H. Lu, S.-K. Mo, P. S. Kirchmann, and Z.-X. Shen, Superconducting graphene sheets in CaC_6 enabled by phonon-mediated interband interactions, *Nat. Commun.* **5**, 3493 (2014).
- [34] G. Savini, A. C. Ferrari, and F. Giustino, First-Principles Prediction of Doped Graphane as a High-Temperature Electron-Phonon Superconductor, *Phys. Rev. Lett.* **105**, 037002 (2010).
- [35] J. C. Tully, Perspective: Nonadiabatic dynamics theory, *J. Chem. Phys.* **137**, 22A301 (2012).
- [36] A. M. Wodtke, J. C. Tully, and D. J. Auerbach, Electronically non-adiabatic interactions of molecules at metal surfaces: Can we trust the Born-Oppenheimer approximation for surface chemistry?, *Int. Rev. Phys. Chem.* **23**, 513 (2004).
- [37] S. Reichardt and L. Wirtz, Nonadiabatic exciton-phonon coupling in raman spectroscopy of layered materials, *Sci. Adv.* **6**, eabb5915 (2020).
- [38] M. J. Bedard-Hearn, F. Sterpone, and P. J. Rossky, Nonadiabatic simulations of exciton dissociation in poly-p-

- phenylenevinylene oligomers, *J. Phys. Chem. A* **114**, 7661 (2010).
- [39] S. Meng and E. Kaxiras, Real-time, local basis-set implementation of time-dependent density functional theory for excited state dynamics simulations, *J. Chem. Phys.* **129**, 054110 (2008).
- [40] C. Lian, S. Hu, M. Guan, and S. Meng, Momentum-resolved TDDFT algorithm in atomic basis for real time tracking of electronic excitation, *J. Chem. Phys.* **149**, 154104 (2018).
- [41] C. Lian, M. Guan, S. Hu, J. Zhang, and S. Meng, Photoexcitation in solids: First-principles quantum simulations by real time TDDFT, *Adv. Theory Simul.* **1**, 1800055 (2018).
- [42] U. D. Giovannini, H. Hübener, S. A. Sato, and A. Rubio, Direct Measurement of Electron-Phonon Coupling with Time-Resolved ARPES, *Phys. Rev. Lett.* **125**, 136401 (2020).
- [43] S. Piscanec, M. Lazzeri, F. Mauri, A. C. Ferrari, and J. Robertson, Kohn Anomalies and Electron-Phonon Interactions in Graphite, *Phys. Rev. Lett.* **93**, 185503 (2004).
- [44] M. Calandra and F. Mauri, Electron-phonon coupling and electron self-energy in electron-doped graphene: Calculation of angular-resolved photoemission spectra, *Phys. Rev. B* **76**, 205411 (2007).
- [45] See Supplemental Material at <http://link.aps.org/supplemental/10.1103/PhysRevB.105.224311> for the details.
- [46] T. Ando, Anomaly of optical phonon in monolayer graphene, *J. Phys. Soc. Jpn.* **75**, 124701 (2006).
- [47] D. Novko, Broken adiabaticity induced by lifshitz transition in MoS₂ and WS₂ single layers, *Commun. Phys.* **3**, 30 (2020).
- [48] For a given doping level, we calculate λ using the same E_f for the adiabatic and nonadiabatic cases, and thus the DOS $N_f \propto E_f$ has the same value in λ . Therefore, the difference in λ with and without nonadiabatic effects only comes from the sum of g_{ii} on different adiabatic FS and NA FS.
- [49] W. L. McMillan, Transition temperature of strong-coupled superconductors, *Phys. Rev.* **167**, 331 (1968).
- [50] P. B. Allen and R. C. Dynes, Transition temperature of strong-coupled superconductors reanalyzed, *Phys. Rev. B* **12**, 905 (1975).
- [51] A. P. Drozdov, M. I. Erements, I. A. Troyan, V. Ksenofontov, and S. I. Shylin, Conventional superconductivity at 203 kelvin at high pressures in the sulfur hydride system, *Nature (London)* **525**, 73 (2015).
- [52] A. P. Drozdov, P. P. Kong, V. S. Minkov, S. P. Besedin, M. A. Kuzovnikov, S. Mozaffari, L. Balicas, F. F. Balakirev, D. E. Graf, V. B. Prakapenka, E. Greenberg, D. A. Knyazev, M. Tkacz, and M. I. Erements, Superconductivity at 250 k in lanthanum hydride under high pressures, *Nature (London)* **569**, 528 (2019).
- [53] J. Kim, C. Jin, B. Chen, H. Cai, T. Zhao, P. Lee, S. Kahn, K. Watanabe, T. Taniguchi, S. Tongay, M. F. Crommie, and F. Wang, Observation of ultralong valley lifetime in WSe₂/MoS₂ heterostructures, *Sci. Adv.* **3**, e1700518 (2017).
- [54] T. Nguyen, F. Han, N. Andrejevic, R. Pablo-Pedro, A. Apte, Y. Tsurimaki, Z. Ding, K. Zhang, A. Alatas, E. E. Alp, S. Chi, J. Fernandez-Baca, M. Matsuda, D. A. Tennant, Y. Zhao, Z. Xu, J. W. Lynn, S. Huang, and M. Li, Topological Singularity Induced Chiral Kohn Anomaly in a Weyl Semimetal, *Phys. Rev. Lett.* **124**, 236401 (2020).